Journal of Power Sources 195 (2010) 6405–6410

Contents lists available at ScienceDirect

Journal of Power Sources

journal homepage: www.elsevier.com/locate/jpowsour

Effects of Nafion loading in anode catalyst inks on the miniature direct formic acid fuel cell

Robert D. Morgan[a], John L. Haan[b], Richard I. Masel[a,*]

[a] Department of Chemical & Biomolecular Engineering, 600 S. Mathews Ave., University of Illinois at Urbana-Champaign, Urbana, IL 61801, USA
[b] Department of Chemistry, 600 S. Mathews Ave., University of Illinois at Urbana-Champaign, Urbana, IL 61801, USA

ARTICLE INFO

Article history:
Received 10 February 2010
Received in revised form 1 April 2010
Accepted 2 April 2010
Available online 9 April 2010

Keywords:
Palladium
Nafion
CO poison
Corrosion

ABSTRACT

Nafion, within the anode and cathode catalyst layers, plays a large role in the performance of fuel cells, especially during the operation of the direct formic acid fuel cell (DFAFC). Nafion affects the proton transfer in the catalyst layers of the fuel cell, and studies presented here show the effects of three different Nafion loadings, 10 wt.%, 30 wt.% and 50 wt.%. Short term voltage–current measurements using the three different loadings show that 30 wt.% Nafion loading in the anode shows the best performance in the miniature, passive DFAFC. Nafion also serves as a binder to help hold the catalyst nanoparticles onto the proton exchange membrane (PEM). The DFAFC anode temporarily needs to be regenerated by raising the anode potential to around 0.8 V vs. RHE to oxidize CO bound to the surface, but the Pourbaix diagram predicts that Pd will corrode at these potentials. We found that an anode loading of 30 wt.% Nafion showed the best stability, of the three Nafion loadings chosen, for reducing the amount of loss of electrochemically active area due to high regeneration potentials. Only 58% of the area was lost after 600 potential cycles in formic acid compared to 96 and 99% for 10 wt.% and 50 wt.% loadings, respectively. Lastly we present cyclic voltammetry data that suggest that the Nafion adds to the production of CO during oxidation of formic acid for 12 h at 0.3 V vs. RHE. The resulting data showed that an increase in CO coverage was observed with increasing Nafion content in the anode catalyst layer.

© 2010 Elsevier B.V. All rights reserved.

1. Introduction

The increasing demand for small, portable electronic devices necessitates the need for the design of small-scale power devices. As a result, batteries and fuel cells have been miniaturized with the goal of maintaining large energy densities. At the present time, fuel cells show an advantage over batteries. Fuel cells are able to maintain a high power density with a decrease in size [1].

Miniature fuel cells are a major contender to replace small-scale batteries and lithium ion batteries in the future. Lithium ion batteries show a drastic reduction in energy density as the total system volume is decreased [2]. As catalysts, membranes and fuel delivery/waste removal systems are optimized, fuel cells could in fact be a lower cost energy source than small-scale batteries.

Complete optimization (finding new membranes or catalysts) is often not needed to show improvement in current fuel cells. For example, simply by changing the thickness of the membrane [3] or composition of the catalyst ink/catalyst layer [4–11], better performance can be achieved. However, a well-designed catalyst layer is the most important aspect of a well-performing fuel cell [12].

The DFAFC is a good choice for miniaturization because it requires virtually no balance of plant components, and it has a high power output compared to other liquid fuel choices, e.g. methanol [13–15]. Although the intrinsic energy content of formic acid is lower than methanol (two electrons per molecule of formic acid vs. six electrons per molecule of methanol), formic acid makes up for this shortcoming, because formic acid can be used in higher concentrations than methanol. This is due to the fact that formic acid has a lower crossover rate than methanol [16–19]. Jeong et al. found that the rate of methanol crossover increases six times as fast as formic acid when compared at the same concentrations [17].

While proton conduction is mainly attributed to the membrane used in the fuel cell, an adequate dispersion of Nafion ionomer must also be present within the catalyst layer to ensure efficient proton conduction to the membrane. Passalacqua et al. studied the distribution of Nafion and the effects on structure and performance of the catalyst layer for hydrogen fuel cells [20,21]. This paper used an illustrative figure to explain why the optimum Nafion loading is not at either extreme of Nafion loadings. At very low Nafion loadings there may be poor proton conduction through the catalyst layer, and there may be low adhesion to the PEM. On the other hand, at high Nafion loadings, there is poor electrical connection between the catalyst particles, and the electron has a difficult time leaving

* Corresponding author. Tel.: +1 217 333 6841; fax: +1 217 333 5052.
E-mail address: r-masel@illinois.edu (R.I. Masel).

0378-7753/$ – see front matter © 2010 Elsevier B.V. All rights reserved.
doi:10.1016/j.jpowsour.2010.04.001

the catalyst layer. While this study was for the hydrogen fuel cell, the qualitative results can still apply to liquid fuel cells.

However, the structure of the anode must be different in a liquid fuel cell. There are two reasons why liquid fuel cells must have a different anode structure. The first reason is the need for the fuel to wet the surface of the catalyst. The second is that while fuel must wet the surface and internal pore structure, there must be adequate room for gaseous products to be removed—CO_2 for the case of methanol and formic acid oxidation [22–24]. Shin found that colloidal Nafion produced the best fuel cell results. This was because the Nafion did not block the pores within the catalyst layer [25]. Tucker et al. showed that a higher pore volume improves the performance of a direct methanol fuel cell (DMFC) [26]. This is likely achieved at lower Nafion loadings, since Poltarzewski et al. showed that at higher Nafion loadings films were observed on the surface [27]. These films would not allow for adequate infusion of the liquid fuel and removal of the gaseous products.

It was shown by Boyer et al. that the proton conductivity of a catalyst layer prepared with Nafion solution is directly proportional to the volume fraction of Nafion within the catalyst layer [28]. Chenitz and Dodelet found that equal volumes of Nafion and palladium gave the best performance in the DFAFC [29]. However, Thomas et al. found that there are benefits having lower Nafion loadings in the catalyst layer. They hypothesized that the lower Nafion loading decreases the thickness of the catalyst layer, which could then allow more catalyst particles to come in contact with the membrane for adequate proton conduction, which would even be enhanced after hot pressing [30]. McGovern et al. found that, upon the addition of Nafion to the surface, the surface areas were suppressed during cyclic voltammetry [31]. The general shape of the CV did not change; however, there was an overall reduction in peak currents. It was determined that Nafion reduces apparent surface area as well as formic acid oxidation current by blocking electrochemically active catalyst sites. Kang et al. studied how Nafion aggregates and processing temperature affected the performance of the fuel cell. The main conclusion from their work was that smaller Nafion aggregates show better catalyst utilization and thus better fuel cell performance [32].

Nafion is, however, a necessary binder for the anodes and cathodes of fuel cells. It is also a strong acid, which can catalyze the dehydration of small organic molecules such as formic acid. In fact, Gates and Schwab published work, which studied the dehydration of formic acid using polystyrene sulfonic acid [33]. Gates found that the polystyrene sulfonic acid could catalyze the dehydration of formic acid directly to CO with no traces of CO_2. This was verified using gas chromatography. Since Nafion is similar to polystyrene sulfonic acid, it too may catalyze the dehydration of formic acid to CO. In addition it has been shown that using 5 M formic acid, no appreciable amounts of CO at 0.3 V vs. RHE accumulate on a palladium surface compared to platinum at the same conditions after 1 h [34].

Here we present our work on three representative Nafion loadings with applications to the miniature DFAFC. We studied the effect of the three different Nafion loadings on fuel cell performance. We also studied how three different Nafion loadings affect electrochemical area loss after potential cycling in formic acid and CO accumulation during constant voltage operation.

2. Experimental methods

2.1. Fabrication of the fuel cells

The fuel cells were fabricated using the method presented in [3]. 25 μm-thick stainless steel plates with 2 mm diameter holes were used as current collectors. Adhesive was transferred to a PDMS puck, and the adhesive was then transferred to the stainless steel foils. A small piece of conditioned Nafion® 117 membrane (Ion Power) was then sandwiched between these two stainless steel plates and the metal–membrane assembly was cured at 110 °C for 20 min. The fuel cell was then hot-pressed at 90 °C for 2 min at an appropriate pressure. The fabricated fuel cell and its dimensions can be seen in Fig. 1.

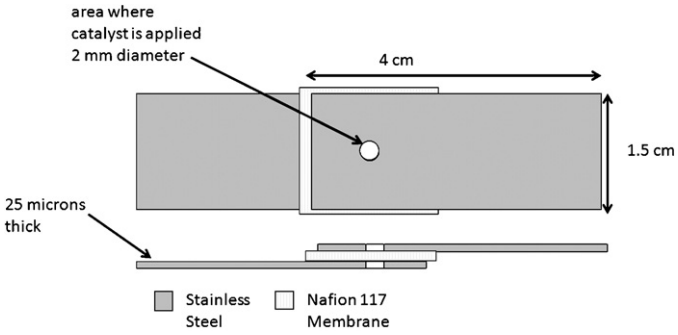

Fig. 1. A top and side view of the assembled stainless steel foils and Nafion membrane. Dimensions are listed where necessary.

2.2. Preparation of catalyst inks for fuel cell

The anode catalyst ink was prepared by mixing Pd black (Aldrich, high surface area) with 5% Nafion solution (Ion Power), 18.2 MΩ Milli-Q water, and isopropanol (Sigma–Aldrich, >99.5%) in an appropriate ratio, and then ultrasonicating the mixture in an ice bath. The cathode ink was prepared in the same manner using Pt black (Alfa Aesar) using the same method. The cathode Nafion content was maintained at 17 wt.%. This was chosen based upon previous work [3] and also the fact that over long periods of times, the anode limits the fuel cell performance [35]. The ink was then applied to the 2 mm diameter exposed Nafion® using the direct paint method. The amount of Nafion in the anode catalyst layer was varied based upon Eq. (1). The values used for the experiments were 10 wt.%, 30 wt.% and 50 wt.%.

$$\text{wt.\% Nafion} = \frac{0.05(\text{mass of Nafion})}{\text{mass of catalyst} + 0.05(\text{mass of Nafion})} \quad (1)$$

The final loadings of the anode and cathode were estimated to be roughly 15 mg cm^{-2}.

2.3. Fuel cell VI testing

All electrochemical measurements were performed at room temperature using a Solartron potentiostat (SI 2187). To obtain VI curves, the cell was placed in a Teflon holder, built in house, as depicted in Fig. 2. The fuel cell was held in the Teflon holder by tightening screws on each corner of the holder. Approximately 1 mL of 12 M formic acid (Fluka, HPLC grade) fuel was placed in the

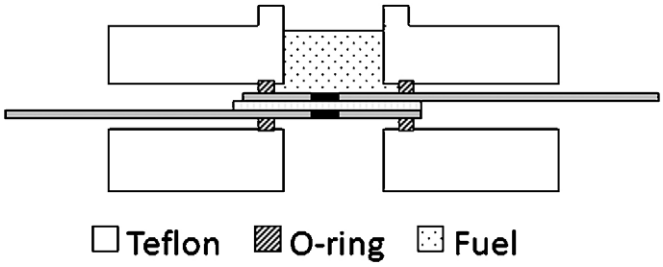

Fig. 2. The fuel cell from Fig. 1 is placed in the Teflon housing for electrochemical testing.

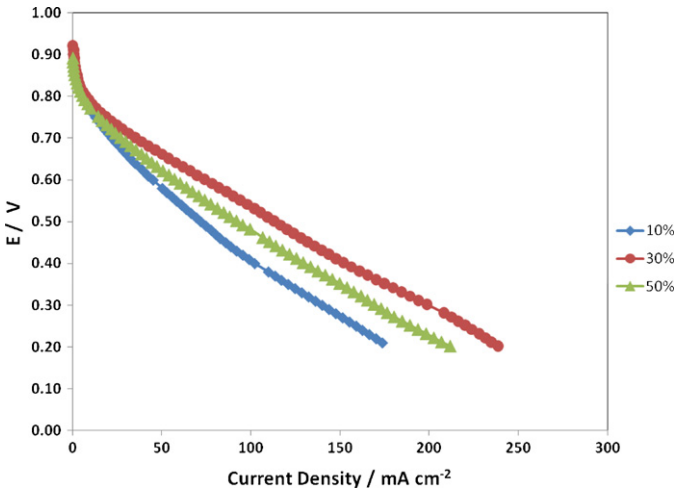

Fig. 3. Polarization curves for the miniature DFAFC showing the performance dependence on Nafion loading in the anode catalyst layer. The Nafion loading in the cathode catalyst layer was maintained at 17 wt.%.

anode reservoir, while the cathode was exposed to quiescent, ambient air. Once a steady open circuit potential was obtained, the VI curve was measured. The potential was stepped from open circuit to 0.1 V. Several VI curves were obtained until the curves stabilized.

2.4. Cyclic voltammetry and chronoamperometry

Because our interest was in isolating the effects of Nafion loading on the fuel cell anode, a standard three-electrode electrochemical cell with Solartron potentiostat (SI 1287) was used for electrochemical measurement. The palladium catalyst ink was made by adding 6 mg Pd black (Aldrich, high surface area), an appropriate amount of Nafion based upon Eq. (1), and 1 g of 18.2 MΩ Milli-Q water. The ink was then ultrasonicated, and 12.5 μL was applied to the tip of a gold electrode. Platinum gauze (Alfa Aesar, 52 mesh woven from 0.1 mm diameter wire, 99.9%) was used as the counter electrode, and a Ag/AgCl/sat'd KCl reference electrode (BAS) was separated from the working electrode via a Luggin capillary. All solutions used were degassed by bubbling high purity argon through them. Cyclic voltammetry in 0.1 M H_2SO_4 (GFS, double distilled) was performed in order to determine electrochemical surface areas by analyzing the area under the hydrogen desorption peaks. The potential was scanned from 0.02 to 1.2 V vs. RHE. Electrochemically active area loss studies were then performed using an electrochemical cell and 12 M formic acid with 0.1 M H_2SO_4. The potentials were scanned between 0.02 and 1.45 V vs. RHE. The sulfuric acid was added to maintain a constant pH to stabilize the reference electrode potential. The working electrode was rotated at 2000 rpm (Princeton Applied Research, Model 616) in order to avoid CO_2 accumulation on the surface. The electrochemically active surface area loss was then characterized by placing the working electrode in a 0.1 M sulfuric acid solution and scanning from 0.02 to 1.2 V vs. RHE. Using the hydrogen desorption peaks, the electro-active area was determined and compared to the areas from before.

For CO build-up studies, initial areas were measured using cyclic voltammograms in 0.1 M H_2SO_4. The working electrode was then placed in 12 M formic acid with 0.1 M H_2SO_4 and rotated at 2000 rpm. The potential was held at 0.3 V vs. RHE for 12 h. The CO adsorbed on the surface was then measured using CO stripping cyclic voltammetry in 0.1 M H_2SO_4 scanning between 0.02 and 1.2 V vs. RHE.

Integration of either the hydrogen peaks or the CO stripping peak can be used to calculate the charge passed for the one or two electron process, respectively. The catalyst oxidation portion of the CV is subtracted from the CO peak resulting in the charge passed only for CO oxidation. It is widely accepted that palladium can be characterized in this manner, where the surface area from the hydrogen peaks is determined from the relationship of 210 μC cm^{-2} and from the CO peaks by the relationship of 420 μC cm^{-2} [36–41].

3. Results and discussion

3.1. Fuel cell results

Fuel cell polarization curves are shown in Fig. 3 using 12 M formic acid as the fuel. It can be seen that the 30 wt.% Nafion cata-

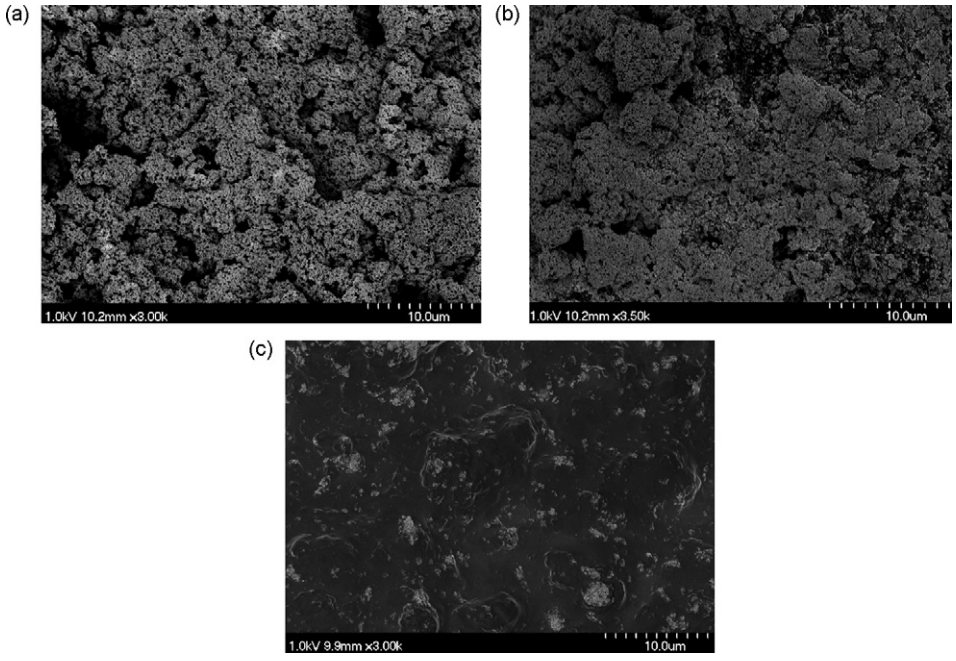

Fig. 4. SEM images showing anode catalyst layers with various Nafion content. (A) Palladium with 10 wt.% Nafion, (B) palladium with 30 wt.% Nafion, (C) palladium with 50 wt.% Nafion.

lyst layer shows the best performance of the three Nafion loadings chosen. Each of the three cases shows very similar open circuit voltages; however, in the high current density region, the 30 wt.% fuel cell has the best performance. These results can be substantiated by examining the SEM (Hitachi S-4700 High Resolution SEM) images of the anode catalyst structures with varying amounts of Nafion. From the SEM images in Fig. 4, it is clear why 50 wt.% Nafion does not show higher performance in the miniature fuel cell. At this level of Nafion loading, there is a Nafion film that forms on the surface of the catalyst layer, which leaves very few exposed catalyst clusters. This was also observed by Poltarzewski et al. [27]. This Nafion film also could offer a mass transfer limitation, which could drastically decrease the performance of the fuel cell. While performance loss in the mass transfer region is not manifested in the miniature DFAFC because the absolute currents are small, it could drastically decrease performance in the larger scale DFAFC where the absolute currents are on the order of amps. Mass transfer limitations would be apparent by using lower concentration formic acid. However, it is not desirable to operate a DFAFC with lower concentrations due to the reduction in fuel energy content. There are also subtle differences between 10 wt.% and 30 wt.% Nafion loading. In the images with 30 wt.% loading, there is enough Nafion for adequate proton conductivity but not so much that it forms a polymer film as in the case of the 50 wt.%. In the 10 wt.% image, there is obviously less Nafion, which may not allow for adequate proton conductivity, which can also be seen by the slight increase of slope in the VI curve of Fig. 3.

3.2. Electrochemical surface area studies

The loss of electrochemical surface area with varying amounts of Nafion in the palladium anode catalyst was investigated by performing potential cycling in 12 M formic acid. In order to isolate the effects of anode composition, the following experiments were done using a three-electrode electrochemical cell. Figs. 5–7 show cycles 1 and 80 of 600 in formic acid for the cases of 10 wt.%, 30 wt.% and 50 wt.% Nafion, respectively. Because the currents of the 600th cycle for each were very small, they were not included in the figures for clarity. Active area is lost in each of the three cases, however, at the completion of the 600 cycles 10 wt.% and 50 wt.% showed the most dramatic loss. To quantify the loss of palladium, the electrochemical surface area before and after cycling in formic acid was measured in 0.1 M H_2SO_4 by cyclic voltammetry. The systems with 10 wt.% and 50 wt.% showed the highest overall loss in area. These were 96 and 99%, respectively. However, for 30 wt.%, the loss in area was only 58%, which is much smaller compared to the other

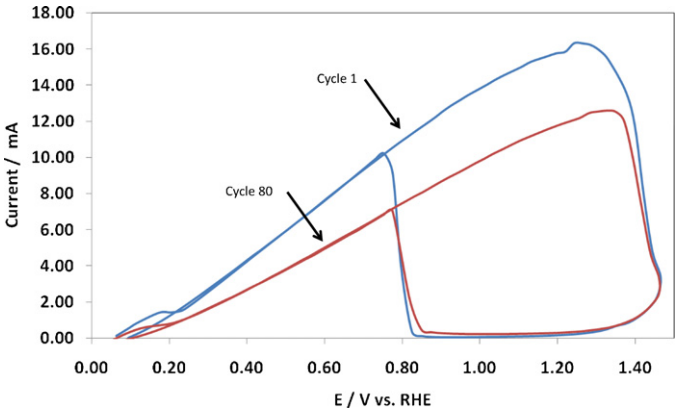

Fig. 6. Cyclic voltammograms for a 30 wt.% Nafion loading showing the loss of activity for cycle 1 and cycle 80 of 600 in 12 M formic acid and 0.1 M H_2SO_4. The scan rate was 50 mV s^{-1}.

two cases. For each system, the potential was scanned from 0.02 to 1.45 V vs. RHE to include portion of the CV that includes the palladium deactivation by surface oxidation. While these potential cycles do not depict what is happening during normal operation of a fuel cell, they do depict what happens during a regeneration step. The formic acid fuel cell produces CO, which is strongly bound to the palladium surface. Due to this poison, the fuel cell must be periodically regenerated by raising the potential of the anode to oxidize the poison. CO is oxidized from the surface at a potential between 0.8 and 0.9 V vs. RHE [42]. However, upon inspection of the Pourbaix diagram, palladium corrodes between 0.8 and 1.2 V vs. RHE at a pH of 1 [43]. Potentials above 1.2 V vs. RHE do not add to the dissolution of Pd. According to the Pourbaix diagram from 1.2 to 1.45 V vs. RHE, palladium is passivated. This can explain why a loss of area during the potential cycles is seen. For the 10 wt.% case, there is little binder to hold the palladium nanoparticles in place during the cycles. This resulted in a large amount of palladium being exposed, which readily dissolved into the solution. For the case of 50 wt.%, there is a thick polymer film which forms over the catalyst layer. This leaves a much smaller number of active sites exposed that are available to do the oxidation reaction. This polymer layer also allows for slower dissolution of the Pd, which explains why in Fig. 7 there is not a substantial loss of activity after 80 cycles. However, only after 600 cycles is the substantial loss observed. While fewer palladium sites may dissolve during the potential cycles, there were far fewer active sites exposed at the beginning of the experiment. For this reason, it can be assumed that a large fraction of the pal-

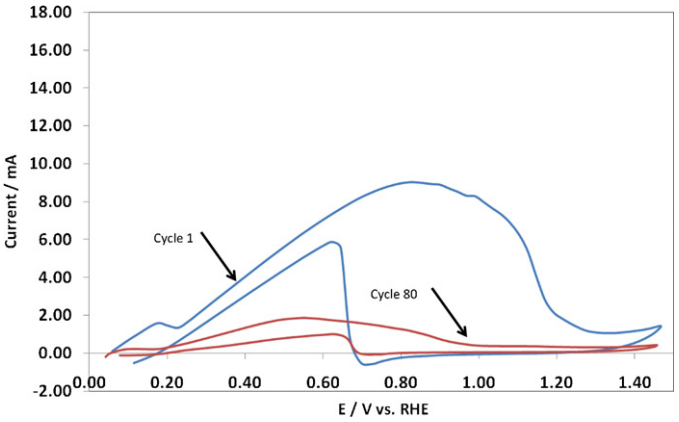

Fig. 5. Cyclic voltammograms for a 10 wt.% Nafion loading showing the loss of activity for cycle 1 and cycle 80 of 600 in 12 M formic acid and 0.1 M H_2SO_4. Cycle 600 lies on the *x*-axis. The scan rate was 50 mV s^{-1}.

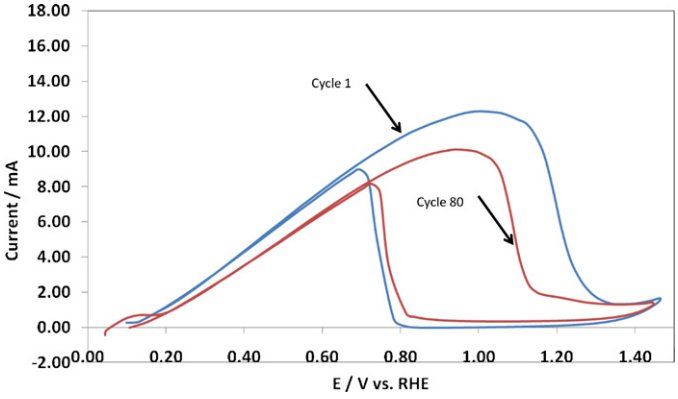

Fig. 7. Cyclic voltammograms for a 50 wt.% Nafion loading showing the loss of activity for cycle 1 and cycle 80 of 600 in 12 M formic acid and 0.1 M H_2SO_4. Due to the polymer film, the dissolution of palladium is slower, and the 99% surface area loss is not manifested until after all 600 cycles. The scan rate was 50 mV s^{-1}.

ladium that was exposed did in fact corrode, which resulted in the 99% loss of area. A 30 wt.% composition was much more stable in terms of area loss than the other two cases. This can be attributed to the fact that there was an adequate amount of binder in the catalyst layer, which did not allow the palladium to readily corrode. However, there was not an overwhelming amount of Nafion to cause the polymer film on the catalyst surface, as in the 50 wt.% loading. Transmission electron microscopy, TEM, was done using a JEOL 2100 Cryo TEM, to determine if particle agglomeration played a major role in the loss of performance. In each of the three cases, the particles grew from 7.5 ± 1.7 nm to 10.6 ± 2.2, 11.8 ± 2.3 and 11.0 ± 2.0 nm, respectively. The final nanoparticle sizes are fairly close, which indicates that particle agglomeration is not the main cause of loss of performance. The major contributing factor to the loss of performance can be attributed to the corrosion of palladium during potential cycling, which is the case during the regeneration step for the DFAFC.

3.3. Catalyst poison build-up studies

Catalyst poison build-up studies were also performed using the same three Nafion compositions, 10 wt.%, 30 wt.% and 50 wt.%. Initial electrochemical surfaces areas were measured using the hydrogen desorption peaks of cyclic voltammograms in 0.1 M H_2SO_4. The initial cyclic scans were also to ensure that the catalyst surface was clean. This was followed by chronoamperometry in 12 M formic acid with 0.1 M H_2SO_4 for 12 h to allow the poison to accumulate on the surface of the palladium. The palladium working electrode was held at 0.3 V vs. RHE to allow CO accumulation, while not allowing any CO to oxidize off the surface. The amount of CO coverage was then characterized by performing further cyclic voltammograms in 0.1 M H_2SO_4. The areas under the CO peak were corrected by subtracting the area under the oxidation portion of the CV, and the hydrogen desorption peaks were then corrected by subtracting the base line due to the double layer charging. These corrected areas were then compared to determine the amount of CO surface coverage. The CO and hydrogen peaks for 10% Nafion loading are shown in Fig. 8. Comparing the areas for these two peaks showed that the CO build-up after the 12 h chronoamperogram lead to a 57% coverage of the electrochemically active surface area. Similar cyclic voltammograms were obtained for 30% and 50% Nafion loadings. They are illustrated in Figs. 9 and 10. By analyzing the CO and hydrogen peaks for these two cases, the coverage was calculated to be 60 and 64%, respectively. There is an apparent trend which shows that as the

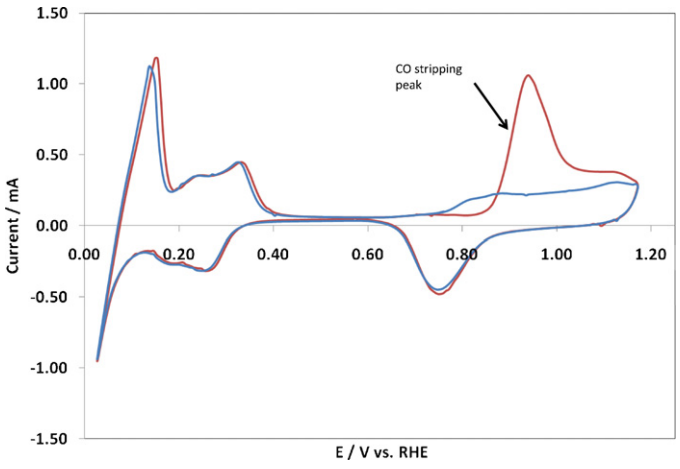

Fig. 8. CO stripping cyclic voltammogram on palladium for 10 wt.% Nafion loading. The scan rate was 10 mV s^{-1}.

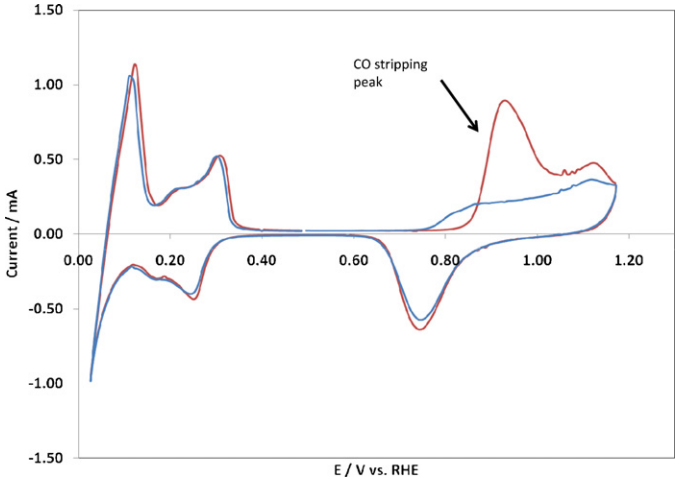

Fig. 9. CO stripping cyclic voltammogram on palladium for 30 wt.% Nafion loading. The scan rate was 10 mV s^{-1}.

Nafion loading is increased there is an increase in the amount of CO present after the chronoamperogram. In order to determine whether this trend was due to Nafion loading or inconsistencies in catalyst preparation, an experiment was performed with only palladium and no Nafion. The cyclic voltammogram obtained is shown in Fig. 11. The resulting CO coverage for the case of just palladium was 32%. While the data show that CO build-up on bare palladium nanoparticles over 12 h in 12 M formic acid does occur, this is drastically less than the CO coverage with Nafion. Although Larsen et al. showed that in 5 M formic acid negligible CO building is observed holding palladium at 0.3 V vs. RHE for 1 h compared to Pt at the same conditions [34], the experiments here used 12 M formic acid and lasted 12 h. Therefore, it is reasonable to expect that there is some CO build-up on the surface. However, the build-up of CO could be enhanced by impurities in the formic acid, such as methyl formate and acetic acid [44,45]. Impurities may enhance the accumulation of CO during constant voltage operation. The impurities, however, do not play a role during potential cycling, because the catalyst reaches potentials sufficient to oxidize the CO from the surface. The data still suggest that there is an additional effect when Nafion is added to the catalyst layer. The increase in CO production with increased Nafion loading aligns well with the observations of Gates. Gates and Schwab reported

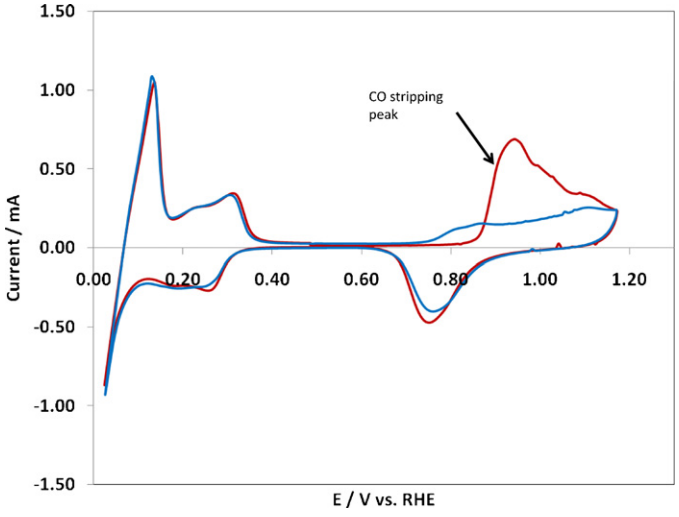

Fig. 10. CO stripping cyclic voltammogram on palladium for 50 wt.% Nafion loading. The scan rate was 10 mV s^{-1}.

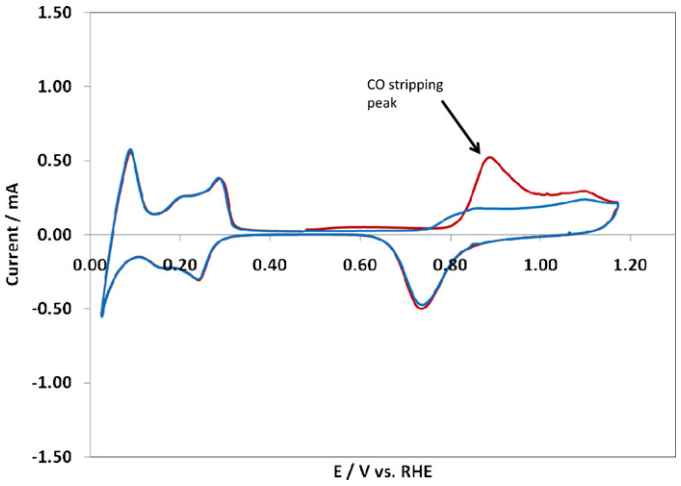

Fig. 11. CO stripping cyclic voltammogram on palladium for 0 wt.% Nafion loading. The scan rate was 10 mV s^{-1}.

that the acid sites in polystyrene sulfonic acid can catalyze the direct dehydration of formic acid to CO [33]. Nafion is a stronger acid than polystyrene sulfonic acid due to the number of fluorines, which withdraw electrons from the sulfonic acid group ($-SO_3^-$). Therefore, Nafion could catalyze the dehydration more readily than polystyrene sulfonic acid. As the Nafion loading is increased, the number of acidic sulfonate sites is also increased. Therefore, there are a greater number of these sites which cause the formic acid dehydration, so as the number of sites is increased, so would the production of CO. This CO could then migrate from the acidic sites within the Nafion to the palladium where it remains strongly bound [35].

4. Conclusions

Several electrochemical methods were used to study the effects of Nafion loading on the direct formic acid fuel cell. Short term fuel cell tests show that 30 wt.% gives the best performance of the three Nafion loadings chosen. This is because it offers a balance between proton conduction and the ability to bind the catalyst. It also does not produce mass transfer limitations. In addition, it was shown that during the regeneration, performance loss can be obtained due to the dissolution of palladium at low pH and high potentials. A loading of 30% Nafion showed the best stability in terms of active area lost after potential cycles. Lastly, it was shown that there is a correlation between CO build-up and the amount of Nafion present in the anode catalyst layer. As the amount of Nafion increases, the amount of CO coverage increases: 57% for a 10% Nafion loading, 60% for a 30% Nafion loading and 64% for a 50% Nafion loading. While these data were obtained with the miniature direct formic acid fuel cell in mind, these results are also applicable for larger scale formic acid fuel cells. Therefore careful consideration needs to be taken when determining the proper amount of Nafion to use.

Acknowledgements

This research was funded by the Defense Advanced Research Projects Agency (DARPA) under grant 2007-0299513-000. Any opinions, findings, and conclusions or recommendations expressed in this manuscript are those of the authors and do not necessarily reflect the views of the US Government. SEM and TEM were carried out in part in the Frederick Seitz Materials Research Laboratory Central Facilities, University of Illinois, which are partially supported by the U.S. Department of Energy under grants DE-FG02-07ER46453 and DE-FG02-07ER46471.

References

[1] S. Moghaddam, E. Pengwang, K.Y. Lin, R.I. Masel, M.A. Shannon, Journal of Microelectromechanical Systems 17 (2008) 1388–1395.
[2] M. Nagata, A. Saraswat, H. Nakahara, H. Yumoto, D.M. Skinlo, K. Takeya, H. Tsukamoto, Journal of Power Sources 146 (2005) 762–765.
[3] H.S. Kim, R.D. Morgan, B. Gurau, R.I. Masel, Journal of Power Sources 188 (2009) 118–121.
[4] D. Lee, S. Hwang, International Journal of Hydrogen Energy 33 (2008) 2790–2794.
[5] S.J. Lee, S. Mukerjee, J. McBreen, Y.W. Rho, Y.T. Kho, T.H. Lee, Electrochimica Acta 43 (1998) 3693–3701.
[6] Y.S. Li, T.S. Zhao, Z.X. Liang, Journal of Power Sources 190 (2009) 223–229.
[7] G. Sasikumar, J.W. Ihm, H. Ryu, Electrochimica Acta 50 (2004) 601–605.
[8] D. Song, Q. Wang, Z. Liu, M. Eikerling, Z. Xie, T. Navessin, S. Holdcroft, Electrochimica Acta 50 (2005) 3347–3358.
[9] J.M. Song, S.Y. Cha, W.M. Lee, Journal of Power Sources 94 (2001) 78–84.
[10] E.A. Ticianelli, J.G. Beery, S. Srinivasan, Journal of Applied Electrochemistry 21 (1991) 597–605.
[11] Z. Xie, T. Navessin, K. Shi, R. Chow, Q. Wang, D. Song, B. Andreaus, M. Eikerling, Z. Liu, S. Holdcroft, Journal of the Electrochemical Society 152 (2005) A1171–A1179.
[12] R. O'Hayre, D.M. Barnett, F.B. Prinz, Journal of the Electrochemical Society 152 (2005) A439–A444.
[13] S. Ha, B. Adams, R.I. Masel, Journal of Power Sources 128 (2004) 119–124.
[14] S. Ha, Z. Dunbar, R.I. Masel, Journal of Power Sources 158 (2006) 129–136.
[15] X. Yu, P.G. Pickup, Journal of Power Sources 182 (2008) 124–132.
[16] B.D. Bath, H.S. White, E.R. Scott, Analytical Chemistry 72 (2000) 433–442.
[17] K.-J. Jeong, C.M. Miesse, J.-H. Choi, J. Lee, J. Han, S.P. Yoon, S.W. Nam, T.-H. Lim, T.G. Lee, Journal of Power Sources 168 (2007) 119–125.
[18] Y.-W. Rhee, S.Y. Ha, R.I. Masel, Journal of Power Sources 117 (2003) 35–38.
[19] X. Wang, J.-M. Hu, I.M. Hsing, Journal of Electroanalytical Chemistry 562 (2004) 73–80.
[20] E. Passalacqua, F. Lufrano, G. Squadrito, A. Patti, L. Giorgi, Electrochimica Acta 43 (1998) 3665–3673.
[21] E. Passalacqua, F. Lufrano, G. Squadrito, A. Patti, L. Giorgi, Electrochimica Acta 46 (2001) 799–805.
[22] S. Uhm, Y. Kwon, S.T. Chung, J. Lee, Electrochimica Acta 53 (2008) 5162–5168.
[23] S. Uhm, J.K. Lee, S.T. Chung, J. Lee, Journal of Industrial and Engineering Chemistry 14 (2008) 493–498.
[24] M. Watanabe, M. Uchida, S. Motoo, Journal of Electroanalytical Chemistry 199 (1986) 311–322.
[25] S.J. Shin, J.K. Lee, H.Y. Ha, S.A. Hong, H.S. Chun, I.H. Oh, Journal of Power Sources 106 (2002) 146–152.
[26] M.C. Tucker, M. Odgaard, P.B. Lund, S. Yde-Andersen, J.O. Thomas, Journal of the Electrochemical Society 152 (2005) A1844–A1850.
[27] Z. Poltarzewski, P. Staiti, V. Alderucci, W. Wieczorek, N. Giordano, Journal of the Electrochemical Society 139 (1992) 761–765.
[28] C. Boyer, S. Gamburzev, O. Velev, S. Srinivasan, A.J. Appleby, Electrochimica Acta 43 (1998) 3703–3709.
[29] R. Chenitz, J.P. Dodelet, ECS Transactions (2008) 647–656.
[30] S.C. Thomas, X. Ren, S. Gottesfeld, Journal of the Electrochemical Society 146 (1999) 4354–4359.
[31] M.S. McGovern, E.C. Garnett, C. Rice, R.I. Masel, A. Wieckowski, Journal of Power Sources 115 (2003) 35–39.
[32] Y. Kang, M. Ren, T. Yuan, Y. Qiao, Z. Zou, H. Yang, Journal of Power Sources 195 (2010) 2649–2652.
[33] B.C. Gates, G.M. Schwab, Journal of Catalysis 15 (1969) 430–434.
[34] R. Larsen, S. Ha, J. Zakzeski, R.I. Masel, Journal of Power Sources 157 (2006) 78–84.
[35] J.L. Haan, K.M. Stafford, R.D. Morgan, R.I. Masel, Electrochimica Acta 55 (2010) 2477–2481.
[36] H. Angerstein-Kozlowska, Comprehensive Treatise on Electrochemistry, Plenum Press, New York, 1984.
[37] T. Biegler, D.A.J. Rand, R. Woods, Journal of Electroanalytical Chemistry 29 (1971) 277–296.
[38] M. Søgaard, M. Odgaard, E.M. Skou, Solid State Ionics 145 (2001) 31–35.
[39] Y. Takasu, T. Kawaguchi, W. Sugimoto, Y. Murakami, Electrochimica Acta 48 (2003) 3861–3868.
[40] P. Waszczuk, T.M. Barnard, C. Rice, R.I. Masel, A. Wieckowski, Electrochemistry Communications 4 (2002) 599–603.
[41] P. Waszczuk, J. Solla-Gullón, H.S. Kim, Y.Y. Tong, V. Montiel, A. Aldaz, A. Wieckowski, Journal of Catalysis 203 (2001) 1–6.
[42] J.L. Haan, R.I. Masel, Electrochimica Acta 54 (2009) 4073–4078.
[43] M. Pourbaix, Atlas of Electrochemical Equilibria in Aqueous Solutions, Pergamon Press Ltd., London, England, 1966.
[44] W.L. Law, A.M. Platt, P.D.C. Wimalaratne, S.L. Blair, Journal of the Electrochemical Society 156 (2009) B553–B557.
[45] R.I. Masel, Y. Zhu, Z. Khan, M. Man, UK. Pat. GB 2,242,650B, 2007.